

EUROPHYSICS LETTERS

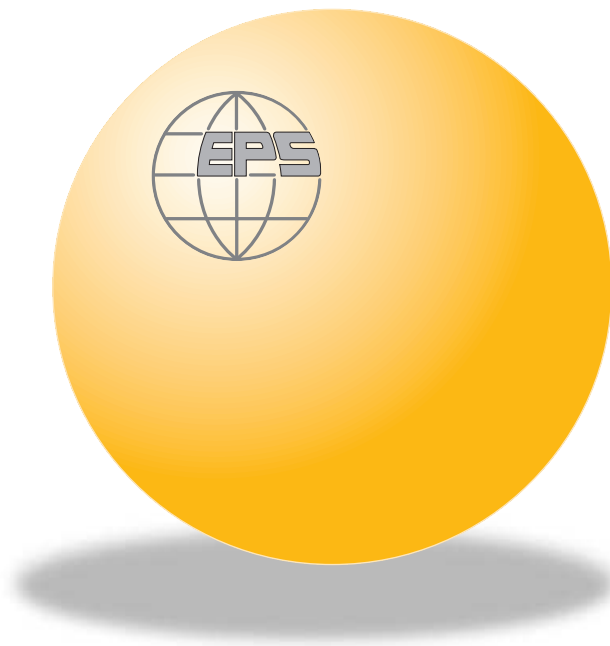
OFFPRINT

Vol. 67 • Number 6 • pp. 1038–1044

Deformation of grain boundaries in polar ice

* * *

G. DURAND, F. GRANER and J. WEISS



Published under the scientific responsibility of the
EUROPEAN PHYSICAL SOCIETY
Incorporating
JOURNAL DE PHYSIQUE LETTRES • LETTERE AL NUOVO CIMENTO

Deformation of grain boundaries in polar ice

G. DURAND¹, F. GRANER^{2(*)} and J. WEISS¹

¹ *Laboratoire de Glaciologie et de Géophysique de l'Environnement
(FRE 2192 CNRS - Université J. Fourier Grenoble 1)
BP 96, F-38402 Saint Martin d'Hères cedex, France*

² *Laboratoire de Spectrométrie Physique
(UMR 5588 CNRS - Université J. Fourier Grenoble 1)
BP 87, F-38402 Saint Martin d'Hères cedex, France*

(received 5 April 2004; accepted in final form 8 July 2004)

PACS. 83.80.Nb – Geological materials: Earth, magma, ice, rocks, etc.

PACS. 81.70.-q – Methods of materials testing and analysis.

PACS. 62.20.Fe – Deformation and plasticity (including yield, ductility, and superplasticity).

Abstract. – The ice microstructure (grain boundaries) is a key feature used to study ice evolution and to investigate past climatic changes. We studied a deep ice core, in Dome Concordia, Antarctica, which records past mechanical deformations. We measured a “texture tensor” which characterizes the pattern geometry and reveals local heterogeneities of deformation along the core. These results question key assumptions of the current models used for dating.

Motivations. – Polar ice cores are the focus of many investigations because they record the history of climatic changes. Owing to snow accumulation, snow-to-ice transformation and slow ice sheet flow ($\sim 10^{-12} \text{ s}^{-1}$), a journey down to the deep layers of the ice sheet is a journey back by several hundred thousands years into the past [1].

A crucial step of paleoclimatic studies from ice cores is dating. In Antarctica, counting annual layers is impossible [2]: absolute dating is only possible for the very top of the ice cores where ice layers containing volcanic impurities can be related to historical volcanic eruptions. Below, dating relies on ice sheet flow models of the evolution of ice layer thinning with depth [2]. Such models are loosely constrained by the identification of large climatic transitions. For the sake of simplicity, these models assume a smooth and monotonous increase of the thinning with depth, hence ignore any possible localization of the deformation [2, 3].

In this letter, we question this essential assumption. We present a method to extract geometrical information (such as thinning, shear, localization of the deformation) from pictures of a cellular pattern using local spatial averages of the “texture tensor” [4]. We apply this analysis to the grain boundaries (the so-called “microstructure”) of ice samples from a deep ice core.

Samples. – Dome Concordia, Antarctica (75° 06' 04'' S, 123° 20' 52'' E, elevation 3233 m a.s.l.) is at the summit of an Antarctic ice dome. It has been chosen because it is usually assumed that the ice flow is axisymmetric around the *in situ* vertical axis, and isotropic within the horizontal plane. In February 2003, the European ice core drilling program (EPICA) reached the depth of 3201.65 m below the ice surface, close to the ground (depth 3309 ± 22 m).

(*) E-mail: graner@ujf-grenoble.fr

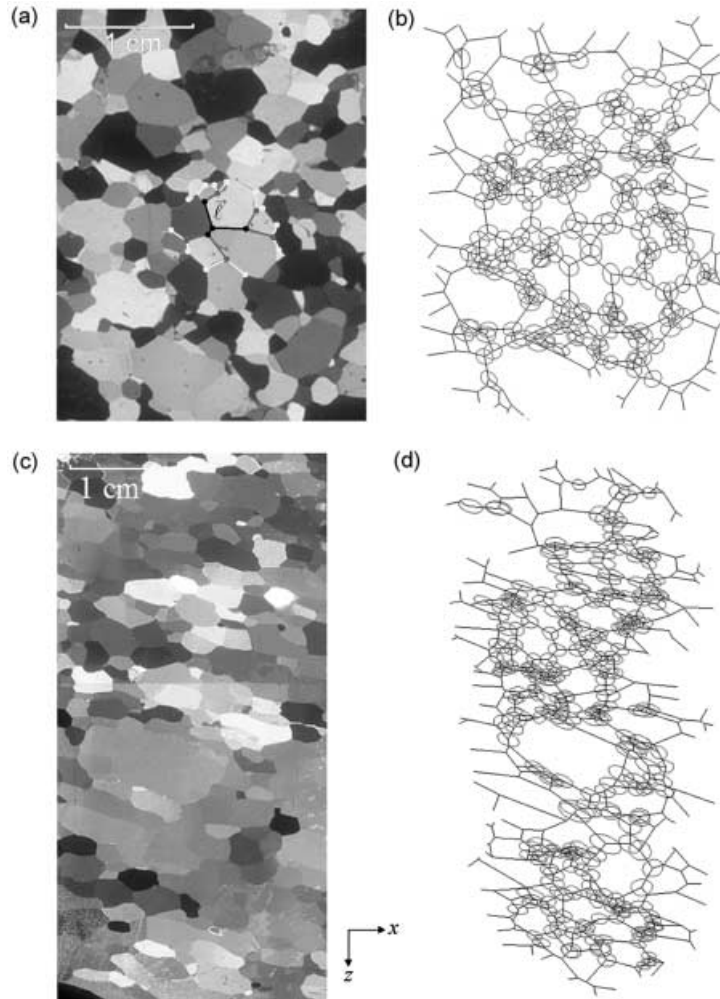


Fig. 1 – Two thin sections of ice imaged between crossed polarizers in white light (a and c) and their corresponding \overline{M} tensor analysis (b and d). Each grain has an almost uniform crystallographic orientation, visualized by its color here represented as grey level. (a) At 362 m depth, the microstructure looks isotropic; (c) at 2629 m depth the microstructure is visibly anisotropic. Superimposed on (a): notations used in the measurement of \overline{M} , here *e.g.* at the site labeled by a black dot. We denote by $\vec{\ell}$ a vector linking it to one of its neighbours. There are 3 such vectors in the first shell, $p = 1$ (black); 6 in shell $p = 2$ (grey); 12 in shell $p = 3$ (white). The texture tensor \overline{M} measured at each site is represented as an ellipse (362 m (b) and 2629 m (d)), with its axes along the eigenvectors, and its half-axes proportional to eigenvalues λ_1, λ_2 , respectively. A site around which the pattern is isotropic is represented by a circle; conversely, a strong anisotropy is represented as an elongated ellipse. The size of the ellipse (same scale for each ellipse) represents the local length of the grain boundaries, *i.e.* quantifies the local grain size. Due to the definition of \overline{M} (eq. (1)), we exclude sites closer than p grains from the image boundary; here $p = 3$.

Samples have been extracted and transported according to standard procedures [5]. We analyzed ~ 11 cm high, ~ 0.1 mm thin sections (fig. 1), with a sampling interval varying from 2 to 25 m. The vertical axis on a thin section always corresponds to the true ice core vertical

axis z ; its horizontal axis, labelled x in what follows, has an unknown and variable orientation within the horizontal plane. The tilt of the core axis from the *in situ* vertical axis was below 0.5° above $z = 2300$ m, then increased up to 5.2° at 3100 m.

Data analysis. – By processing pictures of ice under crossed polarizers, we determine the grain boundaries [5], then the sites (“vertices”) where three boundaries meet, see fig. 1a. For each pair of neighbouring sites, we draw the vector which links them and denote it by $\vec{\ell}$. We then construct the tensor $\vec{\ell} \otimes \vec{\ell}$: its coordinates are $(\ell_i \ell_j)$, where i, j are here x or z ; this tensor is not sensitive to the sign of the vector (it is invariant under $\vec{\ell} \rightarrow -\vec{\ell}$), but it characterizes its length ℓ and its direction.

To statistically characterize the pattern, ref. [4] proposed to define the *texture tensor* $\overline{\overline{M}}$ as the average of $\vec{\ell} \otimes \vec{\ell}$ over a box of fixed size. Such box should be smaller than the image (in order to visualize local details), but still large enough to include a number $N \gg 1$ of wall vectors (to have relevant statistics) [6]. Here, grains have variable size (grains grow with time, hence old grains in deep ice are much larger than young grains near the dome surface): it would be difficult to select such a fixed box size.

We thus chose a local averaging and define $\overline{\overline{M}}$ at each given site as

$$\overline{\overline{M}} = \left\langle \begin{pmatrix} \ell_x^2 & \ell_x \ell_z \\ \ell_z \ell_x & \ell_z^2 \end{pmatrix} \right\rangle_p = \frac{1}{N} \sum_{k=1}^N \vec{\ell}(k) \otimes \vec{\ell}(k) = \mathcal{R} \begin{pmatrix} \lambda_1 & 0 \\ 0 & \lambda_2 \end{pmatrix} \mathcal{R}^{-1}. \quad (1)$$

Here, \mathcal{R} is the rotation which diagonalizes $\overline{\overline{M}}$, and (λ_1, λ_2) are the corresponding eigenvalues; $\langle \cdot \rangle_p$ denotes the average over N vectors, up to the p -th neighbours (fig. 1a). Hence, at each site we include approximately the same number of vectors, $N \approx 3 + 6 + \dots + 3 \times 2^{p-1}$. A smaller p explores local details, a larger p (hence a larger scale) improves the statistics.

This tensor, independent of crystallographic information, does not require any knowledge or hypothesis regarding the past history of the material. The diagonal components M_{xx} and M_{zz} of this tensor are both of order of the average square distance $\langle \ell^2 \rangle$ between sites. Conversely, the off-diagonal component $M_{xz} = M_{zx}$ is much smaller, and even vanishes when the pattern is isotropic. Hence $\lambda_1, \lambda_2 > 0$: the largest eigenvalue corresponds to the direction in which grains are most elongated (figs. 1b and d).

While many other quantitative descriptors exist [7], few are adapted to the determination of the anisotropy of such microstructure pattern. Previous studies on polar ice calculated the aspect ratio of the grains from the linear intercept method [5, 8]. Others used the eigenvalues of the grain inertia tensor [9, 10]; this is a true tensor, with mathematical advantages: for instance, its value does not depend on the particular choice of axes, hence undergoes less artifacts when examining the 2D cut of a 3D pattern.

The tensor $\overline{\overline{M}}$ has the same advantages; but also an additional one, thanks to its definition (eq. (1)) being quadratic in $\vec{\ell}$: it has a physical signification in terms of mechanical deformations [4]. More precisely, its variations (with respect to a reference $\overline{\overline{M}}_0$ measured in an isotropic, relaxed state) define a statistical strain tensor $\overline{\overline{U}}$:

$$\overline{\overline{U}} = \frac{\log(\overline{\overline{M}}) - \log(\overline{\overline{M}}_0)}{2}, \quad (2)$$

which exists even during large deformations and, at least during elastic deformations, coincides with the classical definition of strain [4].

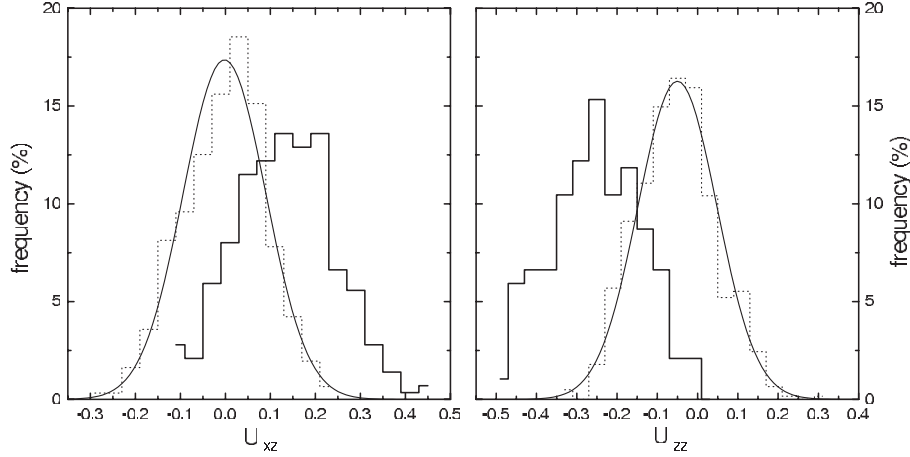


Fig. 2 – Histogram of U_{xz} (left) and of U_{zz} (right) measured with $p = 3$ in fig. 1b: 362 m deep sample (dots), and the corresponding Gaussian distribution (same mean and standard deviation) (thin solid line); and in fig. 1d: 2629 m deep sample (thick solid line).

For the 2D pattern studied here, $\overline{\overline{M_0}}$ is unknown, and processes other than deformation (such as grain growth) modify the microstructure. We first assume that the (viscoplastic) deformation is isochore (incompressibility of ice), so that $\text{Tr} \overline{\overline{U}} = 0$ and $\lambda_1^0 \lambda_2^0 = \lambda_1 \lambda_2$. We also assume that the reference state is isotropic; hence $\overline{\overline{M_0}}$ is isotropic too, so that $\lambda_1^0 = \lambda_2^0 = \sqrt{\lambda_1 \lambda_2}$. We then can measure $\overline{\overline{U}}$ through the following equation:

$$\overline{\overline{U}} = \frac{1}{2} \mathcal{R} \begin{pmatrix} \log \left(\frac{\lambda_1}{\sqrt{\lambda_1 \lambda_2}} \right) & 0 \\ 0 & \log \left(\frac{\lambda_2}{\sqrt{\lambda_1 \lambda_2}} \right) \end{pmatrix} \mathcal{R}^{-1} = \frac{1}{4} \mathcal{R} \begin{pmatrix} \log \left(\frac{\lambda_1}{\lambda_2} \right) & 0 \\ 0 & \log \left(\frac{\lambda_2}{\lambda_1} \right) \end{pmatrix} \mathcal{R}^{-1}. \quad (3)$$

Hence $\overline{\overline{U}}$ has two independent components, U_{zz} and U_{xz} , both largely insensitive to the grain size fluctuations.

To estimate the statistical variability of the measure, we generate 150 isotropic microstructures from a 2D Potts model of normal grain growth [11]. We check that i) each component of $\overline{\overline{U}}$ fluctuates around zero; ii) its distribution is Gaussian (see an example with $p = 3$ in fig. 2); iii) its standard deviation σ only depends on the number N of vectors, *i.e.* on the scale of observation p ; and iv) $\sigma(N) \propto N^{-1/2}$: more precisely, $\sigma \approx 0.34 N^{-1/2}$.

Results. – We first measure the deformation and its heterogeneity within one sample. Figure 1b shows that the upper sample (depth 362 m) is almost homogeneous. Its anisotropy is small and, as expected from a sample taken at a dome, it mainly reflects a uniaxial compression along the vertical axis. Conversely (fig. 1d), the anisotropy of the lower sample, at 2629 m, is stronger; is localized in space; and breaks the axisymmetry around z (see the discussion). This symmetry breaking cannot result from the tilt of the ice core, as the grains are tilted in average by 13.5° from the vertical, much more than the core tilt at 2629 m (2.6°).

Quantitatively, the distributions of U_{xz} (vertical compression) and U_{zz} (horizontal shear) of both samples differ significantly (fig. 2). The upper sample is not sheared ($\langle U_{xz} \rangle = 0.00$), and is slightly flattened onto the horizontal plane ($\langle U_{zz} \rangle = -0.05$). The lower sample is significantly sheared ($\langle U_{xz} \rangle = 0.13$) and strongly flattened ($\langle U_{zz} \rangle = -0.25$). Note that for $p = 3$ ($N = 21$) the intrinsic value of σ (see above) is 0.074; here, the statistical deviation (0.1)

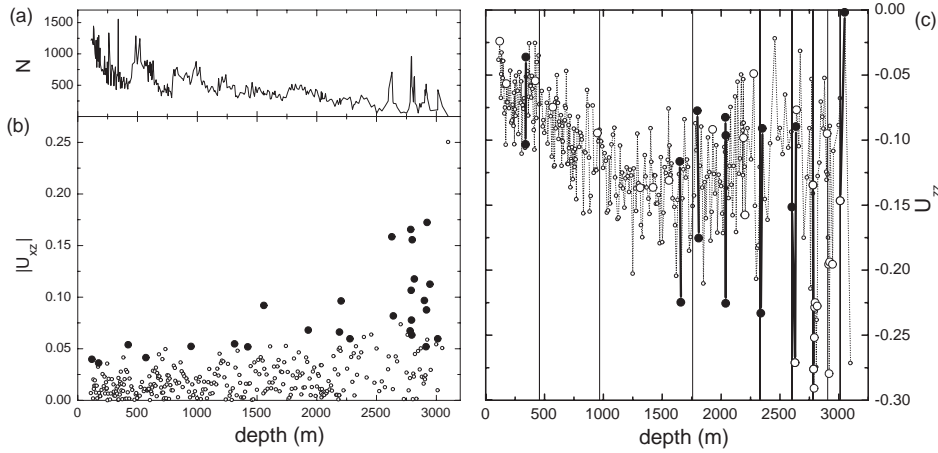


Fig. 3 – Localization of deformation inside the ice core. For each point σ is deduced from the number of vectors N plotted in (a). Each point corresponds to one of 329 samples; same scale for both figures. (b) $|U_{xz}|$ vs. depth. Closed circles highlight samples where $|U_{xz}| > 3\sigma$. (c) U_{zz} vs. depth. Two large closed circles linked by a thick solid line indicate two successive measures which 3σ confidence intervals do not overlap. A large open circle indicates a sample with a large significant shear ($U_{xz} > 3\sigma$, from (b)). Vertical lines indicate zones, associated to climatic transitions, where the grain growth rate changes significantly (see discussion).

is comparable, but slightly larger, reflecting the heterogeneity of deformation at small scales (10^{-2} – 10^{-1} m).

We now turn to heterogeneities at large scale (1 – 10^3 m), by measuring the global $\overline{\overline{U}}$ (integrated over all the grain boundaries of a given sample), vs. the sample depth (fig. 3). Whereas U_{xz} remains around zero, as expected in a dome situation, U_{zz} increases (in absolute value) with depth.

The essential point is the localization: namely, the observation of a deformed (sheared or compressed) layer immediately close to less deformed ones. As mentioned, the grain size increases with depth, therefore the number of vectors per sample decreases (fig. 3a), hence σ increases. The localization is nevertheless significant, and is increasingly frequent at increasing depth (closed circles in figs. 3b and c).

Discussion. – Since the pictures are 2D cuts of actual 3D grains, the apparent average grain size could be misestimated; however, since $\overline{\overline{U}}$ is dimensionless, it should remain unaffected. When, and only when, the pattern is axisymmetric, we can refine the above analysis (eq. (3)). In that case, the eigenvectors are (x, y, z) , and the corresponding eigenvalues are $(\lambda_1, \lambda_1, \lambda_2)$. The eigenvalues of $\overline{\overline{U}}$ are now $\log(\lambda_1/\lambda_2)/6$ and $\log(\lambda_2/\lambda_1)/3$. We have checked that the results corresponding to the 2D analysis (figs. 2, 3) and the 3D one (data not shown) are completely similar, with even slightly more heterogeneities using the latter analysis. Of course, care is required for the interpretation of an individual sheared sample (for instance, regarding U_{zz} at 2629 m, fig. 2b). But on average, the breaking of the axisymmetry hypothesis (large open circles in fig. (3c)) does not introduce significant artifacts on the compression heterogeneities we recorded (closed circles in fig. 3c).

A smooth shear deformation increasing with depth, sampled with a random azimuth, could lead to an apparent heterogeneity of both U_{zz} and U_{xz} . However, this would imply an increasing anisotropy of the microstructure on the horizontal xy plane, whereas six horizontal thin sections were also analyzed (out of 25 available) and showed very small anisotropy (data not

shown). This isotropy of the horizontal thin sections analyzed, combined with the U_{xz} values highlighted in fig. 3b, is actually another expression of strain heterogeneity and of the presence of shear layers. Non-sheared layers, as revealed by isotropic horizontal microstructures, are intercalated with sheared layers revealed by large U_{xz} values (fig. 3b).

Processes such as normal grain growth counteract the anisotropy of grains induced by deformation. Hence the strain recorded by the microstructure \overline{U} underestimates the strain $\overline{\epsilon}$ actually experienced by the material. The growth rate itself could undergo some fluctuations. Near the bottom of the core, a correlation has been observed between small grain sizes (related to a large amount of dust in the ice corresponding to glacial periods [12]) and large strains. In these few cases, highlighted by the thick vertical lines in fig. 3c, the large differences of U_{zz} observed between two adjacent layers could be partly explained by the difference in the grain growth rate. However, this effect is unable to explain most heterogeneities (closed circles in fig. 3c). In addition, it does not explain the large number of shear layers (closed circles in fig. 3b). We note here that such a correlation between grain size and U_{zz} would be difficult to explain in case of a strong effect of a random azimuth. We thus argue that the heterogeneity of anisotropy, observed at both small and large scales, cannot be entirely an observation artifact and has a mechanical origin.

Conclusion and perspectives. – A dating chart is the relation $t(z)$ between depth z and age t of ice: it requires a model, and hypotheses. The ice core is drilled exactly at the summit of a dome, in order to assume that the flow is axisymmetric; so that the ice thinning results from vertical compression only, without horizontal shear. Current models further assume a smooth and monotonous increase of the thinning of ice defined as the ratio $e(z)/e(0)$, where e is the thickness of the annual ice layer at depth z .

The second assumption has already been shown to be wrong in the Greenland ice cores GRIP and GISP2 ([13–15]). Flow disturbances have been reported within at least the 30% deepest part of the GISP2 core, based on the observations of wavy ash layers, crystal striplings visible by unaided eyes, and anomalous fabrics [13]. The dating has been particularly questioned by the observation of a folding, *i.e.* local inversion of ice layers [16].

Here, our method is more accurate and applies to ice itself, without requiring markers nor extreme events. We show that flow disturbances are detectable from almost the top of the ice sheet, and increase in number and intensity with depth. In fact, both dating model assumptions are contradicted by our results: the strain gradient is variable and not even always positive (fig. 3c); and although the flow at a dome is axisymmetric on average, in detail there is a symmetry breaking due to shear, especially in deep layers (fig. 3b). This suggests to reconsider current standard dating charts.

In the future, we expect to correlate the grain boundary pattern with the c -axis orientation, to improve our understanding of their coupling and to elucidate the mechanisms responsible for strain localization.

* * *

We thank M. AUBOUY for his support and useful discussions, M. GLOCK for reading the manuscript, and M. KRINNER and M. MANOUVRIER for their technical support. This work was partially supported by CNRS ATIP 0693. This work is a contribution to the “European project for Ice Coring in Antarctica” (EPICA), a joint ESF (European Science Foundation)/EC scientific program, funded by the European Commission under the Environment and Climate Programme (1994-1998) contract ANV4-CT95-0074 and by national contributions from Belgium, Denmark, France, Germany, Italy, the Netherlands, Norway, Sweden, Switzerland and the United Kingdom.

REFERENCES

- [1] EPICA COMMUNITY, *Nature*, **429** (2004) 623.
- [2] SCHWANDER J., JOUZEL J., HAMMER C. U., PETIT J. R., UDISTI R. and WOLFF E., *Geophys. Res. Lett.*, **28** (2001) 4243.
- [3] HAMMER C. U., CLAUSEN H. B., DANSGAARD W., GUNDESTRUP N., JOHNSEN S. J. and REEH N., *J. Glaciol.*, **20** (1978) 3.
- [4] AUBOUY M., JIANG Y., GLAZIER J. A. and GRANER F., *Granular Matter*, **5** (2003) 67.
- [5] GAY M. and WEISS J., *J. Glaciol.*, **45** (1999) 547.
- [6] ASIPAUSKAS M., AUBOUY M., GLAZIER J. A., GRANER F. and JIANG Y., *Granular Matter*, **5** (2003) 71.
- [7] MECKE K. and STOYAN D. (Editors), *Morphology of Condensed Matter - Physics and Geometry of Spatially Complex Systems*, in *Lect. Notes Phys.*, Vol. **600** (Springer, Heidelberg) 2002.
- [8] ARNAUD L., WEISS J., GAY M. and DUVAL P., *Ann. Glaciol.*, **30** (2000) 8.
- [9] AZUMA N., WANG Y., MORI K., NARITA H., HONDOH T., SHOJI H. and WATANABE O., *Ann. Glaciol.*, **29** (1999) 163.
- [10] WILEN L. A., DIPRINZIO C. L., ALLEY R. B. and AZUMA N., *Microsc. Res. Technol.*, **62** (2003) 2.
- [11] ANDERSON M. P., GREY G. S. and SROLOVITZ D. J., *Philos. Mag. B*, **59** (1989) 293.
- [12] WEISS J., VIDOT J., GAY M., ARNAUD L., DUVAL P. and PETIT J. R., *Ann. Glaciol.*, **35** (2002) 552.
- [13] ALLEY R. B., GOW A. J., MEESE D. A., FITZPATRICK J. J., WASHINGTON E. D. and BOLZAM J. F., *J. Geophys. Res.*, **102** (1997) 26819.
- [14] GOW A. J., MEESE D. A., ALLEY R. B., FITZPATRICK J. J., ANANDAKRISHNAN S., WOODS G. A. and ELDER B. C., *J. Geophys. Res.*, **102** (1997) 26559.
- [15] DAHL-JENSEN D., THORSTEINSSON T., ALLEY R. and SHOJI H., *J. Geophys. Res.*, **102** (1997) 26831.
- [16] GROOTES P. M., STUIVER M., WHITE J. W. C., JOHNSEN S. and JOUZEL J., *Nature*, **366** (1993) 552.